NEUROSCIENCE

Lifelong restructuring of 3D genome architecture in cerebellar granule cells

Longzhi Tan[1,2]*†, Jenny Shi[1,2,3]†, Siavash Moghadami[1,4], Bibudha Parasar[1], Cydney P. Wright[1,5], Yunji Seo[1], Kristen Vallejo[6], Inma Cobos[6], Laramie Duncan[7], Ritchie Chen[2], Karl Deisseroth[2,7,8]*

The cerebellum contains most of the neurons in the human brain and exhibits distinctive modes of development and aging. In this work, by developing our single-cell three-dimensional (3D) genome assay—diploid chromosome conformation capture, or Dip-C—into population-scale (Pop-C) and virus-enriched (vDip-C) modes, we resolved the first 3D genome structures of single cerebellar cells, created life-spanning 3D genome atlases for both humans and mice, and jointly measured transcriptome and chromatin accessibility during development. We found that although the transcriptome and chromatin accessibility of cerebellar granule neurons mature in early postnatal life, 3D genome architecture gradually remodels throughout life, establishing ultra–long-range intrachromosomal contacts and specific interchromosomal contacts that are rarely seen in neurons. These results reveal unexpected evolutionarily conserved molecular processes that underlie distinctive features of neural development and aging across the mammalian life span.

Different cell types within the same organism can mature along highly distinctive developmental and aging trajectories. At the molecular level, cell type–specific gene transcription can be orchestrated by diversity in genome architecture (folding of chromosomes in three dimensions) (*1*). Yet the genome architecture over the life span has not been elucidated, limiting our understanding of the life-spanning cellular dynamics of brain function and dysfunction.

Previously, by using our single-cell three-dimensional (3D) genome assay (diploid chromosome conformation capture, or Dip-C) (*2*–*4*), we found that cells in the mouse forebrain (cerebral cortex and hippocampus) undergo cell type–specific transformation in transcriptome and genome architecture during the first month of life (*5*). However, technological limitation hindered generalization of this finding across brain regions, species, and life span. In this work, we broadened our perspective along all three of these dimensions by turning our focus across the neuraxis—from forebrain to hindbrain—specifically to the cerebellum, which contains ~80% of all neurons in the human brain. The cerebellum, a powerful yet compact processing unit that has expanded over evolution (*6*), exhibits distinct characteristics, including prolonged development after birth, malformation in autism (*7*), and degeneration during aging (*8*). Understanding genome dynamics of the cerebellum may provide insights into these features, as well as into motor control and cognition (*9*).

Prior work has revealed nuclear morphological features of cerebellar cells in vitro (*10*), but the 3D genome structures remain to be fully solved. Recently, chromosome conformation capture (3C or Hi-C) was performed on the adult cerebellum (*11*–*13*); however, a comprehensive, cross-species, single-cell 3D genome atlas of the developing and aging cerebellum is lacking. In addition, simultaneous analysis of transcriptome (*14*) and chromatin accessibility (*15*) in the cerebellum would provide additional valuable information. In this work we show that the cerebellum undergoes an extraordinary, lifelong 3D genome transformation that is conserved between human and mouse and is far greater in magnitude than that of the forebrain (*5*), revealing genome rewiring as a potential molecular hallmark of aging.

A 3D genome atlas of the developing and aging cerebellum

Granule cells (the vast majority of cerebellar neurons) are generated between postnatal days 0 and 21 (P0 and P21) in mice and between the third trimester of pregnancy and ~1 year after birth in humans, which is much later than the same process in the cerebral cortex (*5*). During this period, granule cell progenitors divide and migrate from the external granular layer (EGL) to the internal granular layer (IGL), expanding more than 100-fold in number. Toward the other end of the life span, the cerebellum is also known to exhibit a slow epigenetic aging clock of DNA methylation (*16*). To explore the genomic underpinnings of this entire timeline, we created a 3D genome atlas that extends across the human and mouse life span, alongside a multi-ome atlas focused human development (Fig. 1A).

We first simultaneously profiled transcriptome and chromatin accessibility during postnatal development of the human cerebellum, sequencing 63,768 cells from seven donors (*17*) (one adult and six between the ages of 0.1 and 2.3 years) and detecting a median of 645 to 1617 genes [944 to 3845 unique molecular identifiers (UMIs)] and 12,000 to 34,000 ATAC (assay for transposase-accessible chromatin) fragments per cell from each donor (tables S1 and S2). We additionally profiled a critical age in mouse—P14, when cells are present in both the EGL and the IGL—sequencing 7182 cells and detecting a median of 618 genes (944 UMIs) and 22,000 ATAC fragments per cell.

We then comprehensively profiled 3D genome architecture across the human and mouse life span, sequencing 11,207 cells (Fig. 1A). For humans, we sequenced 5202 cells from 24 donors (0.1 to 86 years) and obtained a median of 608,000 chromatin contacts per cell. Among these cells, 3580 came from the cerebellum (chiefly lateral; vermis if lateral was not available), and 1622 from the cerebral cortex [Brodmann area (BA) 46 of the dorsolateral prefrontal cortex (DLPFC)] of the same donors (tables S2 to S4). For mice, we sequenced 6005 cells from the cerebellum (birth to 21 months), obtaining a median of 496,000 contacts per cell, and incorporated our prior dataset of 1075 and 879 cells from the cerebral cortex and hippocampus, respectively (*5*).

Transcriptionally immature granule cells in the newborn human cerebellum

We integrated the transcriptome dataset from all seven human donors using the LIGER (linked inference of genomic experimental relationships) software (Fig. 1B) (*14*, *18*, *19*); modifying LIGER parameters did not affect conclusions (fig. S1). Granule cells were the predominant cell type at all ages examined (median, 83%; range, 76 to 92%). Astrocytes (median, 7%; range, 3 to 11%) were composed of the cerebellum-specific Bergmann glia (4%) (*18*) and the typical parenchymal astrocytes (2%) (*14*, *15*) (Fig. 1C). We further identified gene *GABRG3* as a specific marker for Bergmann glia (Fig. 1C). Other cell types included molecular layer interneurons (MLIs) (4%), oligodendrocytes (3%), microglia (1%), and unipolar brush cells (UBCs) (0.3%). Purkinje cells were too rare to be reliably identified.

Unlike the case of mouse brain—in which granule cells are almost entirely in the EGL at birth—the human cerebellum is already dominated at birth by IGL neurons. However, it remains unknown when and how human granule cells mature at the genomic level. We found that at birth, granule cells were subdivided into maturation stages by transcriptomic measures (Fig. 1B). In our integrated transcriptome data,

[1]Department of Neurobiology, Stanford University, Stanford, CA 94305, USA. [2]Department of Bioengineering, Stanford University, Stanford, CA 94305, USA. [3]Department of Chemistry, Stanford University, Stanford, CA 94305, USA. [4]Department of Chemical and Systems Biology, Stanford University, Stanford, CA 94305, USA. [5]Department of Biology, Stanford University, Stanford, CA 94305, USA. [6]Department of Pathology, Stanford University, Stanford, CA 94305, USA. [7]Department of Psychiatry and Behavioral Sciences, Stanford University, Stanford, CA 94305, USA. [8]Howard Hughes Medical Institute, Stanford University, Stanford, CA 94305, USA.
***Corresponding author. Email: deissero@stanford.edu (K.D.); tttt@stanford.edu (L.T.)**
†These authors contributed equally to this work.

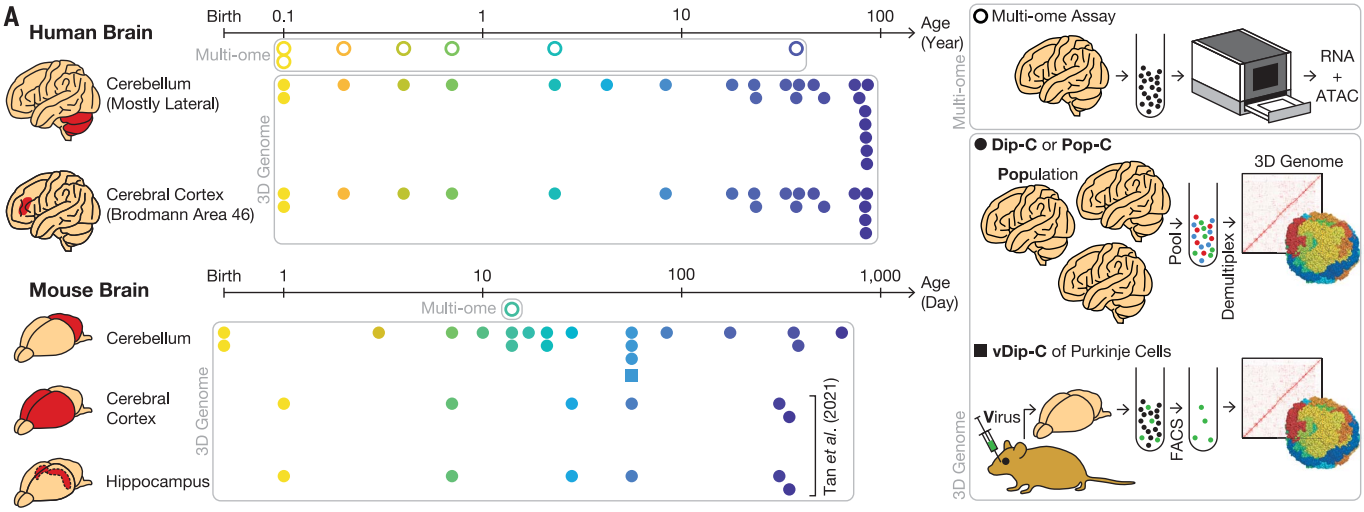

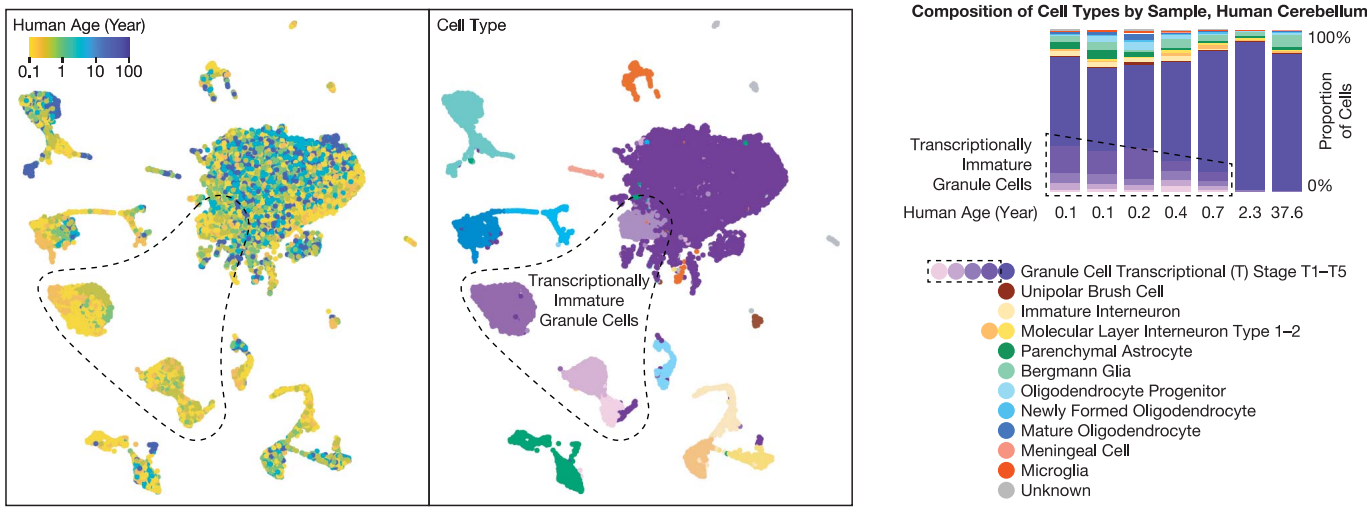

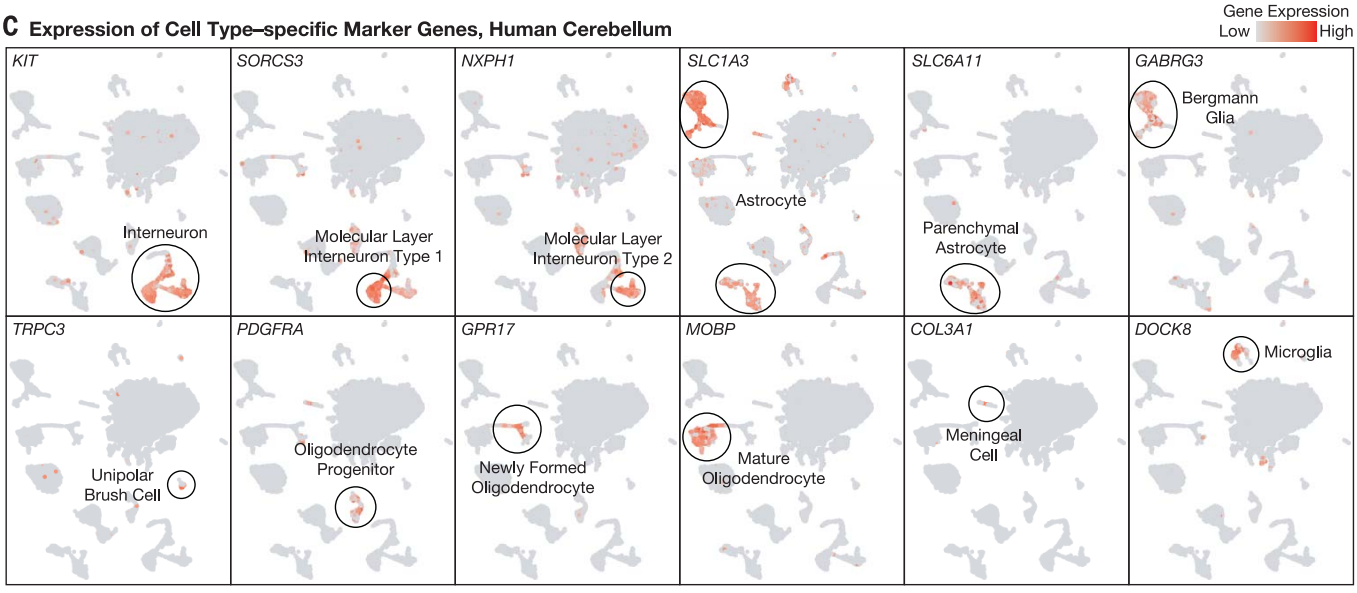

Fig. 1. 3D genome atlas across life span for human and mouse cerebellum with multi-ome atlas of postnatal development. (**A**) Study design. (**B**) Integrative transcriptome analysis of human multi-ome samples. t-SNE, t-distributed stochastic neighbor embedding. (**C**) Representative expression profiles of marker genes.

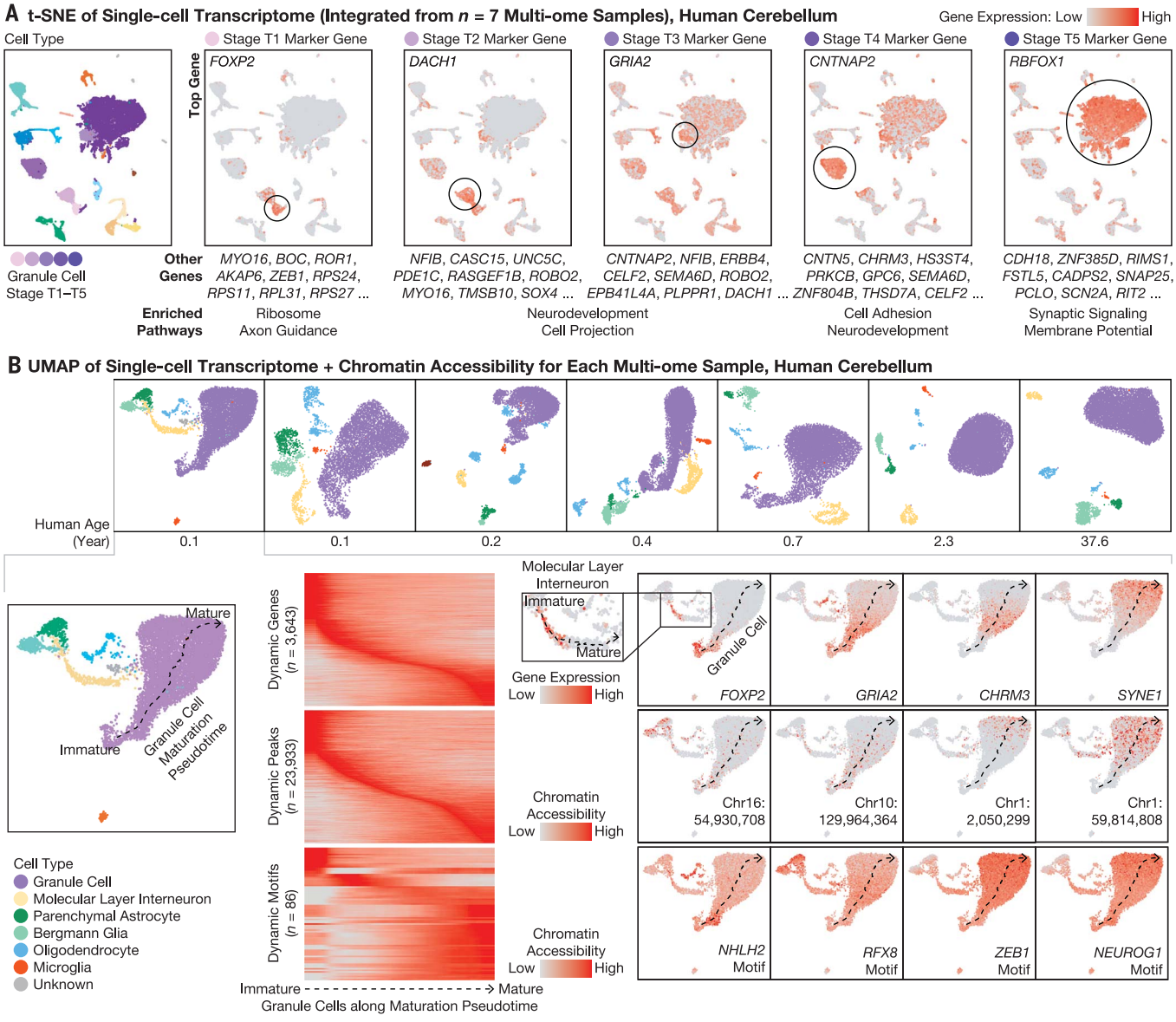

Fig. 2. Simultaneous transcriptome and chromatin accessibility profiling revealed continuous maturation of cerebellar granule cells over the first postnatal year. (**A**) Stages of granule cell maturation, their marker genes (ranked by specificity), and enriched pathways (summarized for the top 100 genes). (**B**) Maturation pseudotime analysis of each sample. *n* = number of dynamic genes, peaks, and motifs. Reference genome, hg38.

granule cells existed in one mature form (termed transcriptional stage T5) and several immature forms (T1 to T4). T5 was the predominant form (99 to 100%) in the 2.3- and 37.6-year-old donors. In younger donors, however, T1 to T4 made up a substantial fraction: 32 to 34% in the 0.1 and 0.2 year olds, 23% in the 0.4 year old, and 14% in the 0.7 year old (Fig. 1B), revealing an abundance of transcriptionally immature granule cells.

T1 to T5 granule cells expressed partially overlapping sets of genes (Fig. 2A and table S5). T1 was enriched for ribosomal subunits [false discovery rate (FDR) < 10^{-10}; including *RPS24/11/27* and *RPL31/39/32*] as well as axon guidance–related genes (FDR = 1×10^{-4}; including *BOC* and *LAMA2*) and expressed *FOXP2*. T2 was enriched for neurodevelopmental genes (FDR = 3×10^{-6}; including *NFIB* and *UNC5C*) including additional genes related to morphogenesis of projections (FDR = 6×10^{-10}; including *ROBO2* and *MYO16*). T3 was also enriched for neurodevelopment (FDR < 10^{-10}; including *ERBB4*) and projection morphogenesis (FDR = 1×10^{-9}; including *SEMA6D*) and expressed *GRIA2*. T4 was enriched for cell adhesion (FDR < 10^{-10}; including *CNTNAP2/5* and *CNTN5*) and genes related to neurodevelopment (FDR = 2×10^{-9}; including *CHRM3* and *GPC6*). T5 was enriched for synaptic signaling genes (FDR < 10^{-10}; including *CADPS2* and *SNAP25*) and regulation of membrane potential (FDR < 10^{-10}; including *RIMS1* and *SCN2A*) and expressed *RBFOX1*. Correlated gene module analysis confirmed these genes and pathways (fig. S3 and table S5).

A continuum of granule cells and interneurons with maturing transcriptome and chromatin accessibility

For each donor, we jointly analyzed transcriptome and chromatin accessibility using ArchR (*20*) (Fig. 2B). Despite discrete appearances in LIGER (Fig. 1A), granule cells formed a continuous developmental pseudotime for each donor below the age of 1 year (figs. S4 and S6A). Dynamically expressed genes included many genes from LIGER analysis. Dynamically accessible transcription factor–binding motifs included ASCL1/2 and NHLH1/2 (early); KLF11/14 and RFX2/3/4/8 (intermediate); and

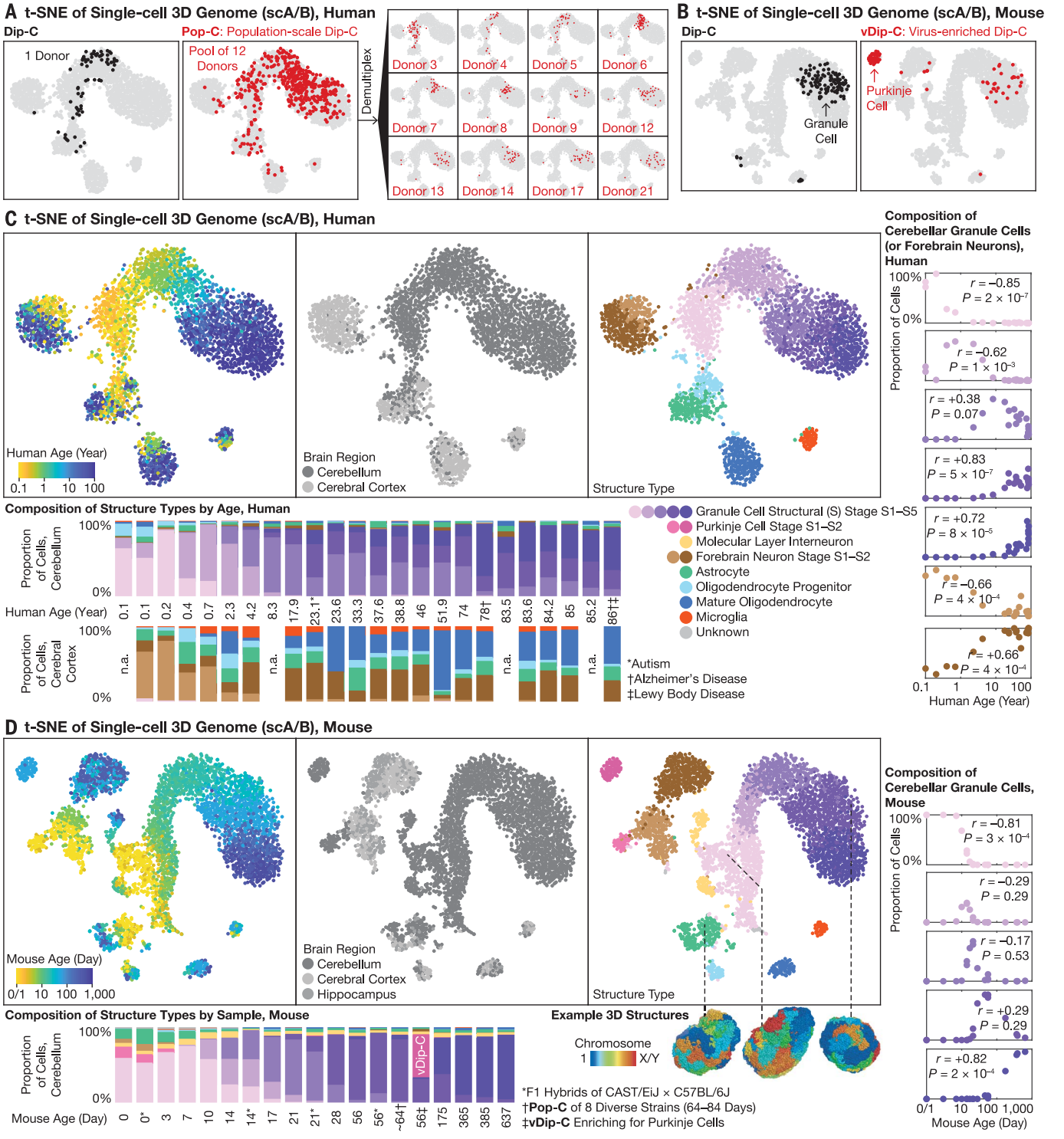

Fig. 3. High-throughput, high-precision 3D genome profiling uncovered lifelong genome remodeling in the human and mouse cerebellum. (**A**) Pop-C method. (**B**) vDip-C method. (**C** and **D**) Cross-species 3D genome atlas for the developing and aging cerebellum (with cerebral cortex as counterpoint). Pearson's *r* (and *P* value) was calculated from logarithm of age.

NEUROG1/2/3, NEUROD4/6, ZEB1, MEF2A/B/C/D, and NFIA/B/X (late). We thus found the newborn human cerebellum to include a complex mixture of granule cells with continuously evolving transcriptomic and epigenomic states. We validated aspects of this continuum by reanalyzing published transcriptome-only data (fig. S6B) (*14*). A continuum was also observed in mouse cells (fig. S7) (*14*).

We observed a similar continuum of maturation in MLIs (fig. S8). Immature MLIs were abundant at birth and vanished over age (64 to 71% in the 0.1 and 0.2 year olds, 44% in the 0.4 year old, 25% in the 0.7 year old, 5% in the 2.3 year old, and <1% in the adult) (Fig. 1B). In addition, immature MLIs and immature granule cells shared expression of many genes, such as *FOXP2* (Fig. 2B).

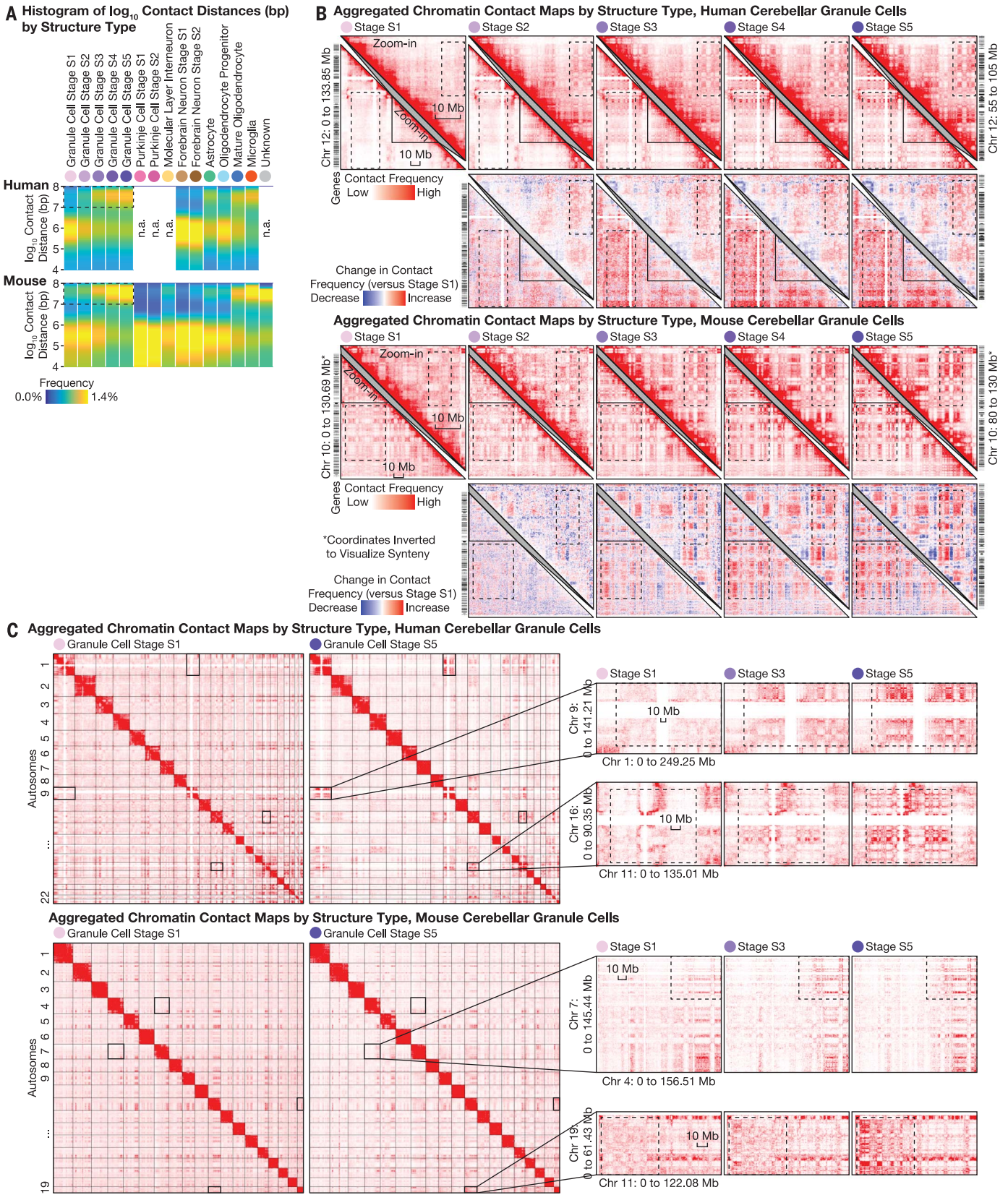

Fig. 4. Cerebellar granule cells formed ultra–long-range intrachromosomal contacts and specific interchromosomal contacts during development and aging. (**A**) Distribution of genomic distances of chromatin contacts. (**B**) Aggregated contact maps for an example chromosome and a zoomed-in region (upper-right triangles). Zoomed-in regions are homologous. Dashed boxes highlight prominent changes. Bin size, 250 kb. Reference genomes, hg19 and mm10. (**C**) Aggregated interchromosomal contact maps. Bin sizes are 6 Mb (human), 5 Mb (mouse), and 500 kb (zoomed-in regions).

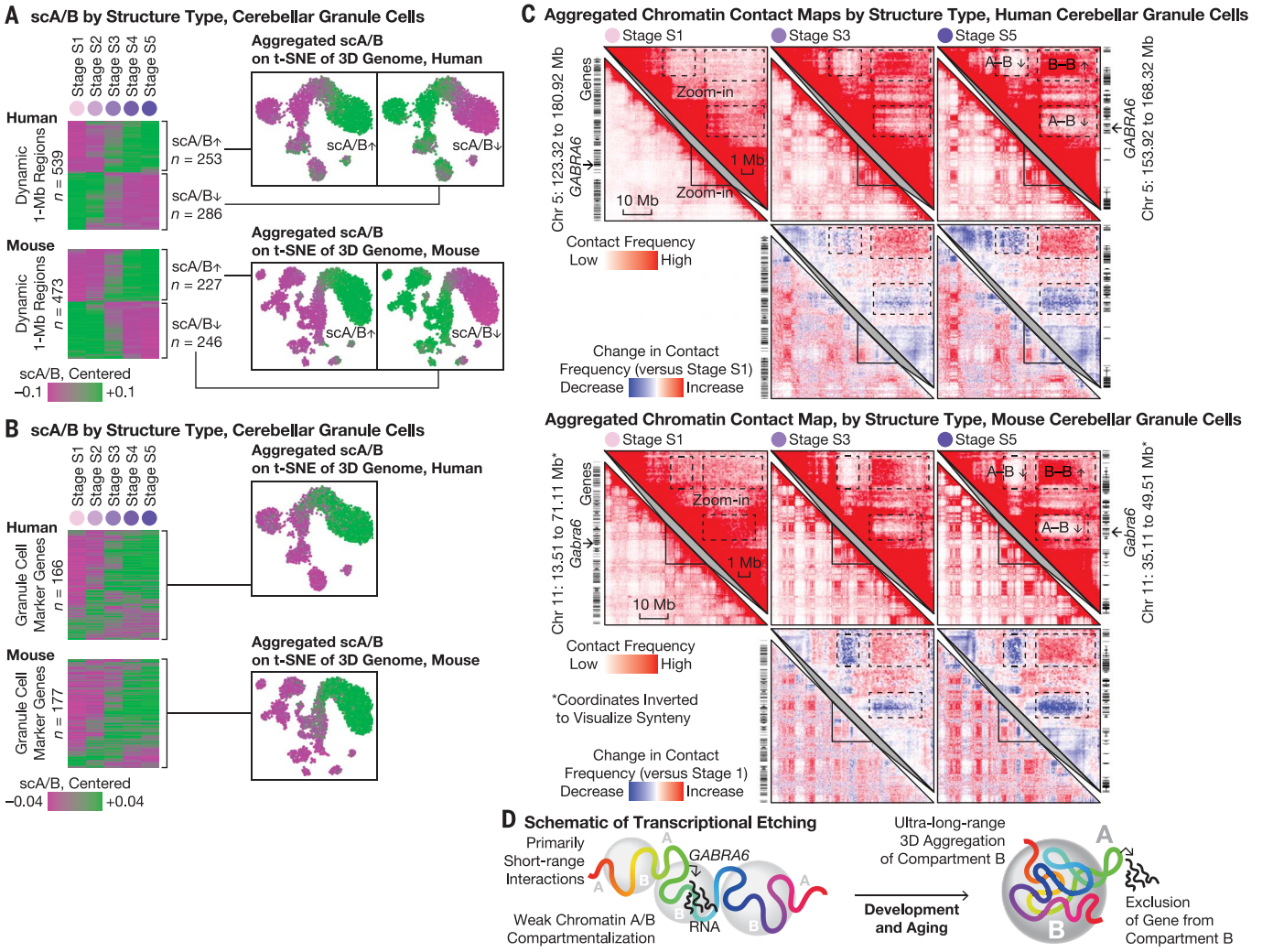

Fig. 5. Lifelong maturation of chromatin A/B compartments was associated with cerebellar granule cell–specific genes. (**A**) Mean scA/B of each dynamic 1-Mb region at each stage (left). Rows are ordered by hierarchical clustering; the two clusters were visualized on t-SNE plots (right). As in (*5*), scA/B calculation excludes contacts within each region and thus primarily reports on long-range interactions. *n* = number of 1-Mb regions. (**B**) (Left) Mean scA/B of each 1-Mb region harboring granule cell–specific marker genes (*14*) at each stage, (right) with aggregated scA/B shown on t-SNE plots. (**C**) Aggregated contact maps for an example gene. Bin size is 100 kb. Reference genomes, hg19 and mm10. (**D**) Schematic of transcriptional etching.

3D genome profiling of diverse populations and rare cells with Pop-C and vDip-C

We next focused on genome architecture. Cerebellar cells exhibit distinct genome morphology, beginning with nuclear dimensions: Granule cell nuclei are among the smallest in the brain (5 to 6 μm in diameter), whereas Purkinje cells have large nuclei (~12 μm in diameter) (*21*). During differentiation, cultured mouse granule cell progenitors reduce nuclear volume and spatially redistribute histone H3.3 (*10*). However, 3D genome structures of cerebellar cells remain unclear, and little is known about lifetime-spanning dynamics in vivo.

To meet this challenge, we developed two 3D genome technologies. First, population-scale Dip-C (Pop-C) leverages the whole-genome sequencing capability of Dip-C (*2*) to pool a large number of samples and computationally demultiplexes (*22*) cells based on natural genetic variations, with high genomic coverage of 10 to 20% (Figs. 1A and 3A). We validated Pop-C by computationally pooling known samples (accuracy, 672/672 = 100%) (fig. S10).

In the simplest case, many of our mouse samples were a pool of males and females, which we demultiplexed based on the ratio of reads between the X chromosome and autosomes (fig. S9). In a more complex case, we pooled one mouse each from the eight founder strains of the JAX Diversity Outbred (DO) collection (*23*) and demultiplexed based on known single-nucleotide polymorphisms (SNPs) (table S4). In the most challenging case, we pooled 3 to 13 unrelated human individuals and demultiplexed them (*22*) based on common SNPs among populations without prior knowledge about donor genotypes (Fig. 3A). Pop-C was thereby shown to provide a robust method for profiling single-cell 3D genome structures at scale (fig. S11).

The second method we developed, vDip-C, enables genomic profiling of rare cell populations without the use of transgenic mouse lines (Figs. 1A and 3B). We used a single viral vector containing a cell type–specific promoter; an ultrabright, fixation-resistant, monomeric fluorescent protein (*24*); and a nuclear membrane localization sequence (*25*) (fig. S12) and administered it to wild-type mice (*26*) through retro-orbital injection of adeno-associated virus (*27*, *28*).

We used vDip-C to solve the 3D genome structures of mouse Purkinje cells (Fig. 3B). Although Purkinje cells are abundant at birth (P0), they quickly become outnumbered by granule cells (Fig. 3D). To isolate this rare (<0.5%)

cell type from adults, we constructed a vDip-C vector with a Purkinje cell–specific promoter (*Pcp2*) (*29*), administered the viral vector to wild-type mice, and isolated nuclei by fluorescence-activated cell sorting (FACS) (fig. S12).

Lifelong 3D genome transformation of granule cells

We created a high-resolution cross-species single-cell 3D genome atlas and resolved 3D genome structures for a subset of cells (from F_1 hybrid mice) (Figs. 1A, 3C, and 3D). Similar to our previous studies (*2*, *3*, *5*), single-cell chromatin A/B compartment (scA/B) analysis revealed 3D genome structure types that corresponded to diverse cerebellar cell types, including granule cells, astrocytes, oligodendrocytes, and microglia in both species, as well as MLIs and Purkinje cells in mice. Replicates yielded reproducible scA/B and contact patterns (Fig. 3A and figs. S11 and S21). Of our 24 donors, three were diagnosed with autism, Alzheimer's disease, and/or Lewy body disease; excluding them did not affect our conclusions (fig. S28).

Granule cells exhibited by far the most dramatic structural transformation. Granule cells of both species were born with an immature structure type, termed structural stage S1, that resembled forebrain neurons (Fig. 3, C and D, and figs. S14 and S19). As the cerebellum developed and aged, granule cells continuously and progressively evolved into new structure types S2 to S5, which increasingly differed from forebrain neurons (figs. S14 and S19). This transformation was the primary source of scA/B variations (the first principal component) and could be visualized regardless of the analysis method (figs. S15 and S16).

In human cells, abundances of S1 to S5 structures peaked around the ages of 0.2, 1, 10, 30, and 80 years, respectively, although considerable between-donor variability was observed (Fig. 3C). This age distribution suggested that S2 to S5 likely all corresponded to T5. In mouse cells, S1 to S5 peaked around P3, P14, P21, P56, and P365, respectively (Fig. 3D); within S5, the 3D genome continued to mature between P365 or P385 (~12 months) and P637 (~21 months) (fig. S17). These data reveal a 3D genome aging clock of large architectural transformation in a mostly postmitotic cell type.

Ultra–long-range intrachromosomal contacts and specific interchromosomal contacts in granule cells

The most prominent architectural changes in granule cells were the emergence of ultra–long-range (10 to 100 Mb) contacts, which had been thought largely restricted to non-neuronal cells (*13*, *30*), except for mouse rod photoreceptors (Fig. 4A) (*3*). From stage S1 to S5, the fraction of contacts that were ≥10 Mb steadily increased from 19 ± 4 to 33 ± 3% in human cells (mean ± SD; two-sided *U* test, $P < 10^{-10}$), and from 19 ± 6 to 34 ± 2% in mouse cells ($P < 10^{-10}$), which were far greater in magnitude than for forebrain neurons [from 15 ± 4 to 16 ± 5% during human development ($P = 0.038$), from 11 ± 4 to 13 ± 3% in mouse cells ($P < 10^{-10}$), and from 9 ± 1 to 10 ± 2% in Purkinje cells ($P = 2 \times 10^{-5}$)] (fig. S18).

This progression in granule cells might be partly driven by their small nuclear size. The abundance of ultra–long-range contacts resembled that seen in non-neuronal cells such as microglia (34 ± 3% in both species) and mature oligodendrocytes (29 ± 4% in human, 27 ± 5% in mouse), both of which have similarly small nuclei. However, these cell types differed substantially in the genomic loci that formed such contacts (fig. S19) and in scA/B profiles (fig. S14), which suggests that nuclear size was not the only driving force.

Granule cells' redistribution of intrachromosomal contacts was accompanied by highly specific interchromosomal contacts. We found increasing interactions among certain human chromosomes, most prominently within a hub of chromosomes (chr) 1, 9, 11, 14, 15, 16, 17, 21, and 22, and between chromosome pairs such as chr 2 and 9, 4 and 14, 8 and 11, and 13 and 20; meanwhile, chr 12 weakened its interactions with the hub (Fig. 4C and fig. S20). Both ultra–long-range intrachromosomal contacts (Fig. 4B) and interchromosomal contacts often involved large stretches of the heterochromatic compartment B interleaved with small stretches of the euchromatic compartment A [also known as "megaloops" or "megaenhancers" (*31*)]. We also observed interchromosomal contacts in mouse cells (Fig. 4C); for example, mouse chr 7 gained interactions with chr 4, 5, 11, 17, and 19. These results highlight another example of conserved, specific interchromosomal interactions beyond prior discoveries in nasal tissue (*3*, *32*–*34*).

Life-spanning scA/B changes associated with granule cell–specific marker genes

Through previous work, we have shown that scA/B generally correlates with cell type–specific gene expression, although discordance can be observed at the single-gene level and regarding temporal dynamics (*3*, *5*). Additionally, it has remained unclear how scA/B interacts with gene expression during aging. In granule cells, we found the predominant mode of scA/B changes to be progressive up- or down-regulation. We calculated the mean scA/B of each 1-Mb genomic region at S1 to S5 and identified the top 20% dynamic regions. In both species, these ~500 dynamic regions either gradually increased or decreased in scA/B across S1 to S5 (Fig. 5A).

We examined genomic regions that harbored conserved marker genes of mature granule cells (*14*). Expression of these ~200 genes began around birth, when T5 emerged. By contrast, on average, these loci gradually increased scA/B throughout life (Fig. 5B and fig. S22). For example, *GABRA6* gradually lost contacts with two nearby heterochromatic regions (which steadily gained contacts with each other) over the life span (Fig. 5C) and consequently increased scA/B until S3 (~10 years) in human cells (two-sided *U* test, $P < 10^{-10}$ from S1 to S2 and 1×10^{-5} from S2 to S3) and until S4 (~P56) in mouse cells ($P < 10^{-10}$ from S1 to S2, 6×10^{-10} from S2 to S3, and 9×10^{-6} from S3 to S4), persisting well after transcriptional up-regulation at ~0.5 years and ~P10, respectively (*14*). Down-regulated genes on average exhibited relatively unchanged scA/B, which was consistent with previous observations (*3*). Increased transcription may continue to etch 3D genome structure long after initial gene activation (Fig. 5D) (*5*).

Robust 3D genome maturation despite functional perturbations

To test the robustness of this genome restructuring, we explored functional perturbation of chromatin remodeling (fig. S26). Using bulk Dip-C, we observed little effect on 3D genome maturation in mice with clinically relevant heterozygous deletion of *Arid1b* (*35*) or *Chd8*, although we cannot rule out more-subtle differences. Granule cell–specific, homozygous deletion of *Chd4* caused moderate 3D changes (*12*); however, these changes had little overlap with (and were much smaller than) our observed architectural maturation.

Discussion

Once born, most neurons must last for a lifetime; however, we know little about how underlying genomic information may be structurally organized. In this work, we discovered distinctive genome architecture in cerebellar granule cells: ultra–long-range contacts that are uncommon in neurons, specific interchromosomal contacts reminiscent of those in nasal tissue (*3*), and restructuring over decades that may be stabilized by cell type–specific gene transcription. We showed that the mouse is an excellent animal model of this process, despite substantial differences from humans in life span.

We provided mechanistic insights into the principles of this reorganization. For example, both granule cells and Purkinje cells lack neuron-specific non-CpG DNA methylation (*13*), revealing that non-CpG methylation was neither required for our previously discovered neuron-specific radial genome movement (*5*)—which we observed in both cell types (fig. S27) (*36*)—nor required for suppressing ultra–long-range contacts.

A potential function of this architecture might be to manage space and energy expenditure. Human brains are 80% cerebellar granule cells by neuron number. If each granule cell consumed the same volume and energy as a typical neuron in the cerebral cortex, metabolic costs could become prohibitive. Consistent with this idea, granule cells are quiet by firing rate (~0.1 Hz) (*37*) compared with

Purkinje cells (~50 Hz) (*38*). Granule cells might therefore have adopted an energy-saving state physiologically, transcriptionally, and architecturally. Cerebellar and hippocampal granule cells adopt different structural strategies despite having similar nomenclature. Hippocampal granule cells were more similar to other forebrain neurons than to cerebellar granule cells (fig. S14) and have larger nuclei (9 to 10 μm in diameter) (*39*, *40*), although both are similarly inactive (firing rates of 0.1 to 0.2 Hz) (*41*). It remains to be determined how granule cells in the olfactory bulb organize their genome.

More broadly, this approach showcases how life-spanning 3D genome profiling of a complex, living tissue can provide unprecedented dimensions of information. This lifelong structural transformation may point the way to previously unidentified therapeutic targets for developmental and aging-related disorders. Wide application of the 3D genome technologies developed here to many brain regions and bodily tissues may contribute to solving long-standing challenges such as dissecting the genetic basis of interindividual variability, characterizing ultrarare cell types, and revealing the full diversity and dynamics of 3D genome organization across the life of mammals.

This study has certain important limitations. For example, we used frozen human samples, which might differ from fresh samples. We also note that vDip-C does not apply to human samples; however, human Purkinje cells could alternatively be isolated by flow cytometry based on size. Future work will be required to test functional relationships between structural and transcriptional changes.

REFERENCES AND NOTES

1. Y. Chi, J. Shi, D. Xing, L. Tan, *Front. Mol. Biosci.* **9**, 959688 (2022).
2. L. Tan, D. Xing, C.-H. Chang, H. Li, X. S. Xie, *Science* **361**, 924–928 (2018).
3. L. Tan, D. Xing, N. Daley, X. S. Xie, *Nat. Struct. Mol. Biol.* **26**, 297–307 (2019).
4. L. Tan, *STAR Protoc.* **2**, 100622 (2021).
5. L. Tan *et al.*, *Cell* **184**, 741–758.e17 (2021).
6. R. A. Barton, C. Venditti, *Curr. Biol.* **24**, 2440–2444 (2014).
7. F. Cauda *et al.*, *J. Neurol. Neurosurg. Psychiatry* **82**, 1304–1313 (2011).
8. C.-Y. Lin, C.-H. Chen, S. E. Tom, S.-H. Kuo; Alzheimer's Disease Neuroimaging Initiative, *Cerebellum* **19**, 217–225 (2020).
9. M. J. Wagner, T. H. Kim, J. Savall, M. J. Schnitzer, L. Luo, *Nature* **544**, 96–100 (2017).
10. D. P. Hoffman *et al.*, *Science* **367**, eaaz5357 (2020).
11. T. Yamada *et al.*, *Nature* **569**, 708–713 (2019).
12. J. V. Goodman *et al.*, *Nat. Commun.* **11**, 3419 (2020).
13. W. Tian *et al.*, Epigenomic complexity of the human brain revealed by single-cell DNA methylomes and 3D genome structures. bioRxiv 2022.11.30.518285 [Preprint] (2022); https://doi.org/10.1101/2022.11.30.518285.
14. M. Sepp *et al.*, Cellular development and evolution of the mammalian cerebellum. bioRxiv 2021.12.20.473443 [Preprint] (2021); https://doi.org/10.1101/2021.12.20.473443.
15. I. Sarropoulos *et al.*, *Science* **373**, eabg4696 (2021).
16. S. Horvath *et al.*, *Aging* **7**, 294–306 (2015).
17. L. Duncan *et al.*, *Neuropsychopharmacology* **48**, 764–772 (2023).
18. V. Kozareva *et al.*, *Nature* **598**, 214–219 (2021).
19. J. D. Welch *et al.*, *Cell* **177**, 1873–1887.e17 (2019).
20. J. M. Granja *et al.*, *Nat. Genet.* **53**, 403–411 (2021).
21. K. S. Bedi, R. Hall, C. A. Davies, J. Dobbing, *J. Comp. Neurol.* **193**, 863–870 (1980).
22. H. Heaton *et al.*, *Nat. Methods* **17**, 615–620 (2020).
23. K. L. Svenson *et al.*, *Genetics* **190**, 437–447 (2012).
24. B. C. Campbell *et al.*, *Proc. Natl. Acad. Sci. U.S.A.* **117**, 30710–30721 (2020).
25. R. J. Platt *et al.*, *Cell* **159**, 440–455 (2014).
26. Q. Huang *et al.*, *PLOS ONE* **14**, e0225206 (2019).
27. K. Y. Chan *et al.*, *Nat. Neurosci.* **20**, 1172–1179 (2017).
28. R. Chen *et al.*, *Nat. Biotechnol.* **39**, 161–164 (2021).
29. K. Nitta, Y. Matsuzaki, A. Konno, H. Hirai, *Mol. Ther. Methods Clin. Dev.* **6**, 159–170 (2017).
30. M. G. Heffel *et al.*, Epigenomic and chromosomal architectural reconfiguration in developing human frontal cortex and hippocampus. bioRxiv 2022.10.07.511350 [Preprint] (2022); https://doi.org/10.1101/2022.10.07.511350.
31. Z. Zhao *et al.*, Mega-Enhancer Bodies Organize Neuronal Long Genes in the Cerebellum. bioRxiv 2023.07.19.549737 [Preprint] (2023); https://doi.org/10.1101/2023.07.19.549737.
32. E. V. Bashkirova *et al.*, *eLife* **12**, RP87445 (2023).
33. K. Monahan, A. Horta, S. Lomvardas, *Nature* **565**, 448–453 (2019).
34. M. Zazhytska *et al.*, *Cell* **185**, 1052–1064.e12 (2022).
35. C. Celen *et al.*, *eLife* **6**, e25730 (2017).
36. Y. Takei *et al.*, High-resolution spatial multi-omics reveals cell-type specific nuclear compartments. bioRxiv 2023.05.07.539762 [Preprint] (2023); https://doi.org/10.1101/2023.05.07.539762.
37. K. Powell, A. Mathy, I. Duguid, M. Häusser, *eLife* **4**, e07290 (2015).
38. M. Arancillo, J. J. White, T. Lin, T. L. Stay, R. V. Sillitoe, *J. Neurophysiol.* **113**, 578–591 (2015).
39. E. Gagyi *et al.*, *Brain Pathol.* **22**, 803–810 (2012).
40. K. S. Bedi, *J. Comp. Neurol.* **311**, 425–433 (1991).
41. Y. Senzai, G. Buzsáki, *Neuron* **93**, 691–704.e5 (2017).

ACKNOWLEDGMENTS

We thank Arima for early kit access; NIMH HBCC, Stanford ADRC, and NIH NeuroBioBank for human samples; F. Zhang (MIT) and X. Jin (Scripps) for advice on *Chd8* and KASH; C. Celen (UT Southwestern) for help on *Arid1b*; H. Heaton (Auburn) for advice on souporcell; R. Corces (UCSF) for help with ArchR; D. Xing (Peking), J. Raymond (Stanford), T. Clandinin (Stanford), A. Brunet (Stanford), L. Fan (Stanford), and P. Wang (Stanford) for helpful discussion; students of SIN bootcamp (J. Bendrick, J. Cheng, C. Lewis, K. Malacon, N. Manfred, and B. Zhou) for help on experiments; Stanford PAN; and Stanford Shared FACS. We thank donors and their families, medical examiners offices, UMBTB, and SMRI brain bank for contribution to HBCC. **Funding:** BWF CASI, Baxter Foundation, Stanford MCHRI Uytengsu-Hamilton Award, Stanford Medicine Dean's Fellowship, and Stanford Berry Fellowship (L.T.); Stanford Chemistry, Stanford Bio-X, Goldwater Foundation, and Stanford Major Grant (J.S.); Stanford Barres Fellowship (B.P.); Stanford NeURO Fellowship (C.P.W.); NIH/NIA P30 AG066515 and CZI 2019-199150 (I.C.); NIMH R01 MH123486, NIMH R21 MH125358, and Stanford Jaswa Award (L.D.); NINDS K99 NS119784 (R.C.); and Gatsby Foundation and NIH (K.D.). **Author contributions:** Experiment design: L.T., J.S., I.C., L.D., R.C., and K.D.; Experiment performance: L.T., J.S., B.P., K.V., and R.C.; Data analysis: L.T., J.S., S.M., C.P.W., B.P., Y.S., K.V., I.C., L.D., R.C., and K.D.; Writing: L.T. and K.D. **Competing interests:** L.T. is an inventor on the Dip-C patent US 11,530,436 ("Multiplex end-tagging amplification of nucleic acids"). K.D. is a cofounder and a scientific advisory board member of Stellaromics and Maplight Therapeutics and a scientific advisory board member of BrightMinds Biosciences. **Data and materials availability:** Raw and processed data are available under the BioProject PRJNA933352 (https://www.ncbi.nlm.nih.gov/bioproject/?term=PRJNA933352). Code is available from GitHub (https://github.com/tanlongzhi/dip-c). The vDip-C vector is available from Addgene (https://www.addgene.org/207613).

SUPPLEMENTARY MATERIALS

science.org/doi/10.1126/science.adh3253
Materials and Methods
Figs. S1 to S28
Tables S1 to S6
References (*42*–*54*)

Submitted 25 February 2023; accepted 3 August 2023
10.1126/science.adh3253

Lifelong restructuring of 3D genome architecture in cerebellar granule cells

Longzhi Tan, Jenny Shi, Siavash Moghadami, Bibudha Parasar, Cydney P. Wright, Yunji Seo, Kristen Vallejo, Inma Cobos, Laramie Duncan, Ritchie Chen, and Karl Deisseroth

Science, **381** (6662), .
DOI: 10.1126/science.adh3253

Editor's summary

Containing nearly half of the neurons in the brain, the cerebellum is one of its most neuron-dense areas. Tan *et al*. performed transcriptome and chromatin accessibility analysis at different developmental stages in human and mouse cerebellar granule cells (see the Perspective by Akbarian and Won). The authors describe the main differences between human and mouse granule cells, but also point out that both show continuous modulation of genome architecture throughout life. These results provide valuable insights into granule cell changes during development and aging. —Mattia Maroso